Terrestrial myriametric radio burst observed by IMAGE and Geotail satellites

Shing F. Fung,[1] Kozo Hashimoto,[2] Hirotsugu Kojima,[2] Scott A. Boardsen,[3,4] Leonard N. Garcia,[5] Hiroshi Matsumoto,[6] James L. Green,[7] and Bodo W. Reinisch[8]

Received 16 July 2012; revised 13 January 2013; accepted 23 January 2013; published 15 March 2013.

[1] We report the simultaneous detection of a terrestrial myriametric radio burst (TMRB) by IMAGE and Geotail on 19 August 2001. The TMRB was confined in time (0830–1006 UT) and frequency (12–50 kHz). Comparisons with all known nonthermal myriametric radiation components reveal that the TMRB might be a distinct radiation with a source that is unrelated to the previously known radiation. Considerations of beaming from spin-modulation analysis and observing satellite and source locations suggest that the TMRB may have a fan beamlike radiation pattern emitted by a discrete, dayside source located along the poleward edge of magnetospheric cusp field lines. TMRB responsiveness to IMF Bz and By orientations suggests that a possible source of the TMRB could be due to dayside magnetic reconnection instigated by northward interplanetary field condition.

Citation: Fung, S. F., K. Hashimoto, H. Kojima, S. A. Boardsen, L. N. Garcia, H. Matsumoto, J. L. Green, and B. W. Reinisch (2013), Terrestrial myriametric radio burst observed by IMAGE and Geotail satellites, *J. Geophys. Res. Space Physics*, *118*, 1101–1111, doi:10.1002/jgra.50149.

1. Introduction

[2] Myriametric radio emissions (with wavelengths of 10–100 km) from Earth's magnetosphere have been known to take on different forms [e.g., *Green and Fung*, 2005]. Most notable forms include the classical nonthermal continuum (NTC) with both escaping and trapped components [*Gurnett*, 1975; *Gough*, 1982; *Green and Boardsen*, 1999; *Menietti et al.*, 2005], continuum enhancement (CE) [*Gough*, 1982; *Filbert and Kellogg*, 1989; *Kasaba et al.*, 1998], and auroral myriametric radiation (AMR) [*Hashimoto et al.*, 1994]. One type of continuum radiation emanating from plasmaspheric notches at the magnetic equator can sometimes extend to higher frequencies (up to ~800 kHz) to form the so-called kilometric continuum (KC) radiation [*Hashimoto et al.*, 1999]. CE has also been known to appear as low-frequency bursts associated with substorm particle injections. This paper presents the first observations of a terrestrial myriametric radio burst (TMRB) that was detected simultaneously by IMAGE and Geotail at 0832–0952 UT on 19 August 2001, although the observations by Geotail lasted a little longer (0830–1006 UT). The widely separated satellite observations at 12–50 kHz suggest that the TMRB was a temporal event. We will compare the TMRB observations with the characteristics of other known TMR components to determine if the TMRB may be consistent with any of the known TMR.

2. Observations of TMRB

2.1. Spacecraft Locations

[3] The IMAGE and Geotail satellites were widely separated during the times of TMRB observations. IMAGE was in a 1.15-by-8.2 R_E polar orbit with a period of ~14.2 h. The IMAGE spacecraft was spinning nominally at 0.5 rpm like a reverse cartwheel along its orbit. On the other hand, the Geotail spacecraft was in a 9-by-30 R_E low-inclination orbit with the spin axis making an angle of 87° to the ecliptic plane, an orbital period of ~5.3 days, and a spin rate of 20 rpm.

[4] On 19 August 2001, 0830–1006 UT, the IMAGE satellite was near apogee ($R \sim 8$ *Re*) over the northern polar region in the afternoon sector, while Geotail was at perigee ($R \sim 9$ *Re*) located just north of the magnetic equator in the post-midnight/pre-dawn sector. Using the NASA SSCWeb tool (http://sscweb.gsfc.nasa.gov), we show in Figure 1 the IMAGE and Geotail positions projected onto the GSM *X-Y* plane during the times of TMRB observations. The IMAGE and Geotail GSM coordinates indicate that the two satellites were situated on opposite sides of Earth, nearly along an afternoon–early morning meridian plane. IMAGE, however, was at much-higher geomagnetic

[1]Geospace Physics Laboratory, NASA Goddard Space Flight Center, Greenbelt, Maryland, USA.
[2]Research Institute for Sustainable Humanosphere, Kyoto University, Kyoto, Japan.
[3]Heliophysics Science Division, NASA Goddard Space Flight Center, Greenbelt, Maryland, USA.
[4]Goddard Planetary Heliophysics Institute, University of Maryland, Baltimore, Maryland, USA.
[5]Wyle, NASA Goddard Space Flight Center, Greenbelt, Maryland, USA.
[6]Headquarters, Kyoto University, Kyoto, Japan.
[7]Planetary Science Division, NASA Headquarters, Washington, District of Columbia, USA.
[8]Lowell Digisonde International, Lowell, Massachusetts, USA.

Corresponding author: S. F. Fung, Geospace Physics Laboratory, NASA Goddard Space Flight Center, Greenbelt, MD, USA. (shing.f.fung@nasa.gov)

2169-9380/13/10.1002/jgra.50149

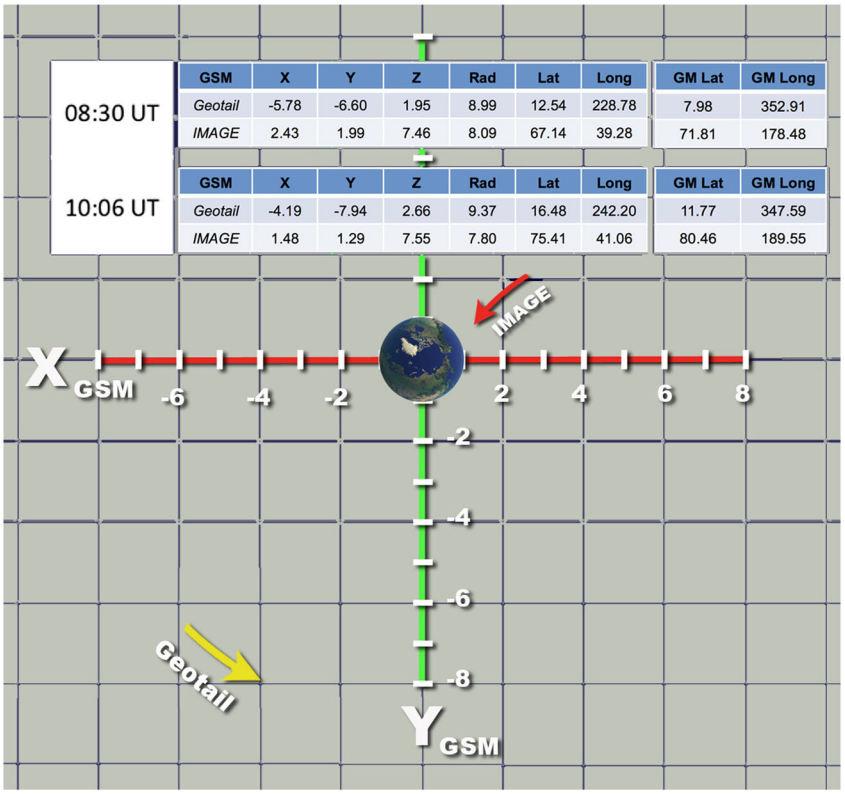

Figure 1. *X-Y* plane projections of the GSM positions (in R_E) and geomagnetic (GM) latitudes and longitudes of IMAGE (red) and Geotail (yellow) over the interval of TMRB observations at 0830–1006 UT on 19 August 2001. The two satellites were at different geomagnetic latitudes on opposite sides of the earth (LT ~14.6 and ~3.3, respectively), both at the time in the northern hemisphere with increasing Z_{GSM}. The arrowheads indicate the projected directions of the satellite orbital motions.

latitudes (71.81º–80.46º) than Geotail (7.98º-11.77º). The difference in geomagnetic longitudes shown in Figure 1 means that the two satellites are situated on nearly diametrically opposite sides of a meridian plane. Over this interval, the geomagnetic longitude of IMAGE increased by ~11º, while that of Geotail decreased by ~5.3º.

2.2. IMAGE and Geotail Observations

[5] The IMAGE Radio Plasma Imager (RPI) [*Reinisch et al*., 2000] operations alternated between passive radio wave measurements and active radio sounding measurements. The passive observations were accomplished by two consecutive measurement programs: one operating at 3–20 kHz in 42 linear frequency steps and another one at 20–1000 kHz in 199 steps of 2% increment. While it took ~1 min to complete both passive measurement programs, these passive observations were typically repeated only every ~4–5 min, depending on the time, orbital position, and the number of intervening active measurement operations. On the other hand, it takes only 8 s to step through 128 frequency steps in the 12.5–100 kHz band of the Plasma Wave Instrument (PWI) [*Matsumoto et al*., 1994] on Geotail, which has been in continuous operations since launch in July 1992.

[6] Figure 2 shows the 6 h dynamic spectrograms for 19 August 2001, recorded by the IMAGE RPI (lower panel) and Geotail PWI (upper panel). The emission feature in the frequency range of 12–50 kHz observed simultaneously by both satellites at 0832–0952 UT is identified here as the TMRB. We should note that the color scales of the two spectrograms are not readily comparable because the two data sets are not intercalibrated and the signal strength quantities being plotted are not the same. Given the widely separated spacecraft locations, the simultaneous observations of the TMRB by both satellites strongly suggest that the TMRB was turning on and off, just like a light bulb.

[7] In view of the large differences in the IMAGE and Geotail latitudes and longitudes, it is of interest to contrast the wave signatures between the two spectrograms in Figure 2. First, the TMRB observed by both satellites appears as an isolated magnetospheric emission with an intensity enhancement peak near ~0900 UT. The simultaneous observations of the TMRB, when IMAGE and Geotail were fortuitously located at very different latitudes on nearly diametrically opposite sides of the Earth, suggest that the TMRB must have a radiation pattern that could be broad in latitude but could also be confined meridionally. These characteristics give a possible appearance of at least an instantaneous fan-beam pattern that covers the latitude and longitude ranges of both IMAGE and Geotail. As we will discuss later, the rarity of simultaneous, multispacecraft observations of TMRB events and the lack of temporally extended (more than few hours) TMRB emissions that are distinct from other TMR components tend to argue against TMRB as being broadly beamed in longitude. Beaming characteristics of TMRB are detailed later in section 6.

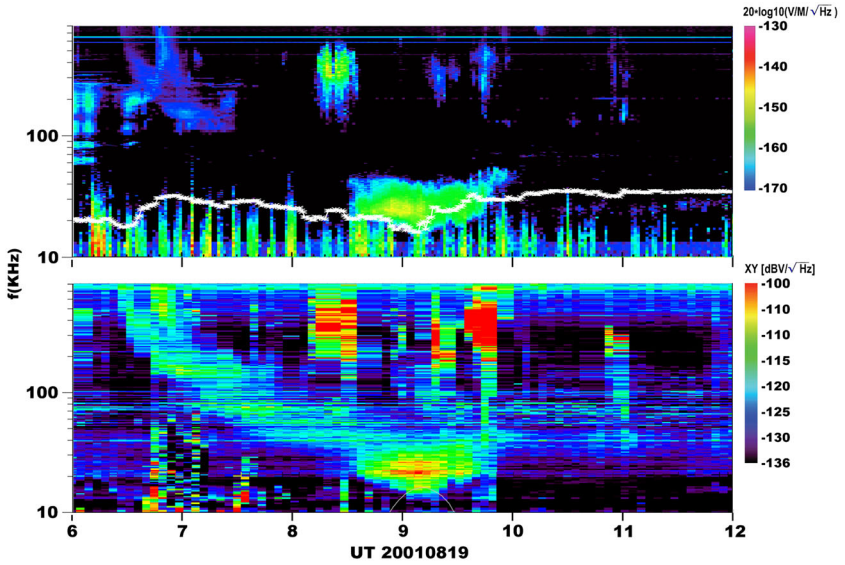

Figure 2. A 6 h data interval on 19 August 2001 showing the isolated TMRB observed by IMAGE at 0832–0952 UT on the dayside at high latitude (lower panel) and Geotail at 0830–1006 UT on the nightside at low latitude (upper panel). Geotail's observation of the TMRB at frequencies below the solar wind electron plasma frequency (white trace in the upper panel) after 0910 UT strongly suggests that the TMRB radiation was beamed directly from a magnetospheric source.

[8] Both IMAGE and Geotail also detected several of the same solar type III bursts. One burst was seen (starting just before 0700 UT) by IMAGE to have a low-frequency dispersive tail that extends to the TMRB (Figure 2, lower panel), although no such tail was detected by Geotail (Figure 2, upper panel). The absence of the type III tail at Geotail may be due to its position at the time being deep in the nightside magnetosphere (see Figure 1) and that the low-frequency tail (below ~100 kHz) might have been blocked by the intervening plasmasphere. The type III tail seen at IMAGE, however, means that the solar wind density at the time must have been sufficiently low to allow the tail emission to be detected by IMAGE. The solar wind plasma frequencies from OMNI data (white trace in the upper panel of Figure 2) do show a near match of the lower cutoff of the first half of the TMRB, but they quickly exceeded the TMRB lower cutoff throughout the rest of the burst. This behavior essentially rules out the possibility of a solar wind source for the TMRB.

[9] The TMRB was observed simultaneously by IMAGE and Geotail at widely different positions. It was observed over similar myriametric frequency ranges, with IMAGE RPI at 13.5–36.5 kHz and Geotail at 12.5–60 kHz. Despite the slight frequency differences, both sets of observations show that the TMRB had a lower cutoff frequency that decreased toward the center from both the beginning and end of the burst. The frequency bandwidth is also broadest near the center of the burst where Geotail observations extended to slightly lower frequencies. Both sets of observations show an intensity enhancement near ~0900 UT (i.e., 0900 UT for Geotail and 0910 UT for IMAGE) and distinct upper and lower frequency cutoff profiles with no evidence of other background myriametric emissions. The TMRB spectral characteristics observed by both IMAGE and Geotail thus argue that it is a distinct magnetospheric emission.

[10] Figure 3 shows an expanded view of the last hour of the TMRB in Geotail data (see upper panel of Figure 2). The clearly spin-modulated burst signals shown in Figure 3 imply that the TMRB radiation had well-defined direction of propagation and was beamed directly from its source, although no such spin modulation was seen by IMAGE RPI due to the much slower satellite spin rate (0.5 rpm) and a longer time (~ 1 min) to complete a frequency scan. The tapered shape of the frequency-time profile toward the end of the burst, particularly in the lower cutoff frequencies, is quite evident and consistent with the IMAGE observations shown in Figure 2 (lower panel). The upper cutoff frequencies nearing ~60 kHz, on the other hand, exhibit a number of cycles of undulations, as if the source densities were going through a series of enhancements and depletions. The undulation period is about 5 min, which corresponds to a frequency of ~3.3 mHz, i.e., similar to a Pc5 wave frequency.

3. TMRB Source Direction by Spin-Modulation Analysis

[11] The spin-modulated TMRB signals (shown in Figure 3) observed by Geotail provide an excellent opportunity for determining the directions of arrival of the signals as

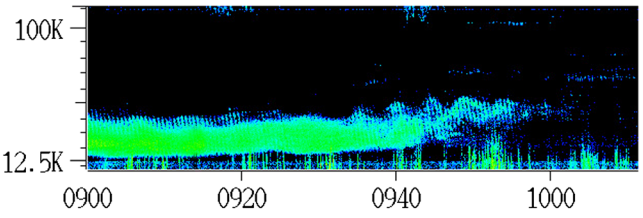

Figure 3. A portion of the Geotail observations covering the end of the TMRB at 1006 UT, showing clear spin-modulated emissions with the typical interference-like pattern and the unusual undulating upper cutoff frequencies that occurred throughout the TMRB event.

seen from Geotail, and thus the potential for determining the source location. Spin modulation occurs when a rotating wire antenna intercepts an arbitrarily polarized, transverse electromagnetic radiation that is propagating in a relatively fixed direction. The antenna would register a minimum intensity when the wire antenna is oriented mostly along the signal propagation direction, and a maximum intensity when it is oriented transversely with respect to the signal propagation direction. If the frequency-scan time is longer than the spacecraft (i.e., antenna) spin period, successive intensity minima and maxima would result at regular frequency and time intervals, resulting in an interference-like intensity pattern that is characteristic of spin-modulated signals [*Scarf et al*., 1968]. The degree of spin modulation can be reduced if (1) the wave propagation direction is tilted with respect to the antenna spin plane, or (2) the incoming waves have mixed directions of propagation. The latter case can occur if the arriving signals are made up of radiation from multiple source points or an extended source.

[12] Figure 3 shows that the degree of spin modulation does vary over frequency and time within the TMRB. Upon close examination, however, Figure 3 also reveals that except for certain discrete time intervals when the TMRB was obviously contaminated by locally occurring low-frequency broadband electrostatic noise, both the upper and lower frequency edges of the TMRB show consistent spin modulations. The low noise background at the lower TMRB cutoff frequencies reflects the spin-modulation pattern quite clearly, particularly at times when the broadband noise is absent (e.g., at times shortly before both 0920 and 0940 UT). The spin modulations also appear throughout the burst over the whole TMRB frequency range without evidence of other contaminating emissions (such as due to reflected signals or other background radiation), particularly before 0840 UT (not shown) and after 0940 UT.

[13] Following the procedures of *Hashimoto et al*. [1999], we have determined the Geotail antenna directions during certain times and frequencies at which spin-modulated TMRB intensity minima (and maxima) are observed. The degree of spin modulation, expressed in terms of a modulation index [e.g., *Fainberg*, 1979; *Menietti et al*., 1998], is measured by fitting a cosine curve to a 160 s observation interval at a fixed frequency. The azimuthal source direction projected onto the antenna spin plane and modulation index at a given time are obtained by taking the average of those quantities for five different neighboring frequency channels for that time. Figure 4 shows the results of our direction-finding analysis performed at nine different times (labeled 1–9 at 10 min increments) during the TMRB interval.

[14] The small blue circles in Figure 4 mark the Geotail GSE positions at the different times when spin-modulation analyses were performed. The red segments represent the directions to the TMRB source as seen from the different Geotail orbital positions, and the green segments mark the directions to the center of the Earth as seen from Geotail at different magnetic local times, from ~3:10 to ~4:10.

[15] The red segments in Figure 4 clearly show that the TMRB radiation, when projected onto the GSE *X-Y* (Geotail antenna-spin) plane, appeared to arrive at Geotail on average from an earthward azimuthal direction (i.e., not sunward along positive-X_{GSE}). As such, the TMRB source could still be located off the GSE *X-Y* plane, either on the nightside or over the pole on the dayside. The different directions of arrival are distinct despite the finite uncertainties involved (represented by the circular arcs), and show that there is a systematic change in the directions of arrival from 1 to 9. The change in Geotail orbital positions notwithstanding, a dayside (nightside) TMRB source clearly moved toward earlier (later) local times during the 80 min interval over which spin-modulation analyses were performed. This change in the source direction with time, including the momentary shift of the direction in step 7 (0930 UT) back toward later (earlier) local times (as in steps 1 and 2), appears to be physical. We will further explore and discuss the TMRB beaming and source characteristics in section 6.

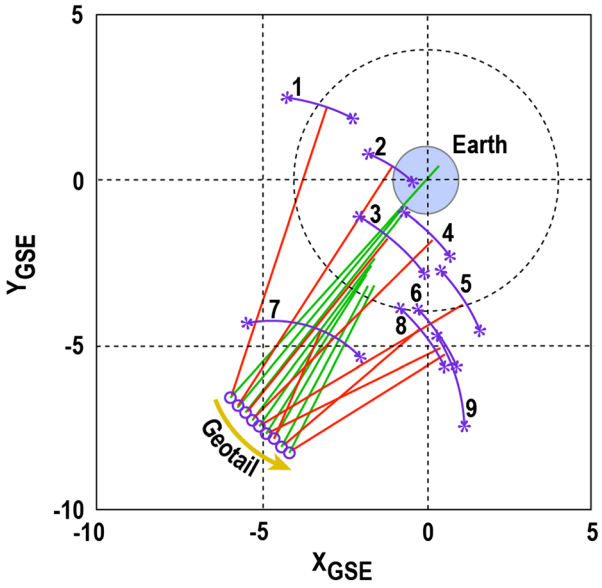

Figure 4. Direction-finding analysis of spin-modulated TMRB observations at nine successive times (labeled 1–9), each separated by 10 min, from 0830 to 0950 UT at selected frequencies between 38 and 47 kHz. Shown in the Geotail spin plane (GSE *X-Y*), the green lines are parallel to the directions toward the center of the earth as seen from the instantaneous Geotail positions, and the red lines represent the nominal TMRB source directions having uncertainties given by the corresponding circular arcs. The length of each red (and associated green) line segment at each time step (Geotail position) indicates the spin-modulation index [*Fainberg*, 1979]. The solid and dotted circles mark Earth and the 4 *Re* boundary, respectively.

[16] While the orientations of the red and green segments represent different directions, their lengths (which are the same for the same observation time) represent the degrees of spin modulation seen at different Geotail positions. They should not, however, be confused with distances to the TMRB source locations. If a segment length of 10 *Re* represents a modulation index of 100%, then the (red and green) segment lengths in Figure 4 show a systematic change in the modulation indices ($M = 93$, 86, 69, 78, 73, 60, 36, 47, and 57%) as a function of time during the TMRB interval, during which Geotail actually moved slightly southward in GSE latitude from $-9°$ to $-10.5°$, even though it was moving northward in GSM and GM coordinates as shown in Figure 1.

4. Solar Wind and Magnetospheric Conditions Associated With the TMRB

[17] A number of terrestrial myriametric radiation components are known to be dependent on geomagnetic activity. It is therefore of interest to see what solar wind and geomagnetic conditions are associated with the TMRB emission.

4.1. Solar Wind and IMF Conditions

[18] Figure 5 plots the 1 min solar wind, interplanetary, and auroral activity data obtained from the NASA OMNIWeb (http://omniweb.gsfc.nasa.gov). The top 5 panels in Figure 5 show the external magnetospheric driver parameters: the interplanetary magnetic field (IMF) strength (|***B***|); the IMF Bx, By, and Bz components (in GSM); and the solar wind speed, respectively. These parameters show no remarkable upstream activity up to 1 h before and during the entire TMRB interval, over which we have $4 <$ IMF $|B| < 7$ nT and $+2 <$ IMF $Bz < +7$ nT. Throughout the entire interval (0700–1100 UT) encompassing the TMRB event, the solar wind speed in fact decreased rather steadily from 490 km s^{-1} at 0700 UT to 450 km s^{-1} at 0900 UT, and then increased again to about 480 km s^{-1} at 1000 UT before leveling off afterward. With limited observations, it is not clear at the present time if decreased solar wind speed plays any role in the TMRB emission process.

[19] The positive IMF Bz condition throughout the interval, however, may be of significance because such condition can lead to magnetic reconnection over limited region poleward (or tailward) of the cusp (particularly with IMF $Bx < 0$ as

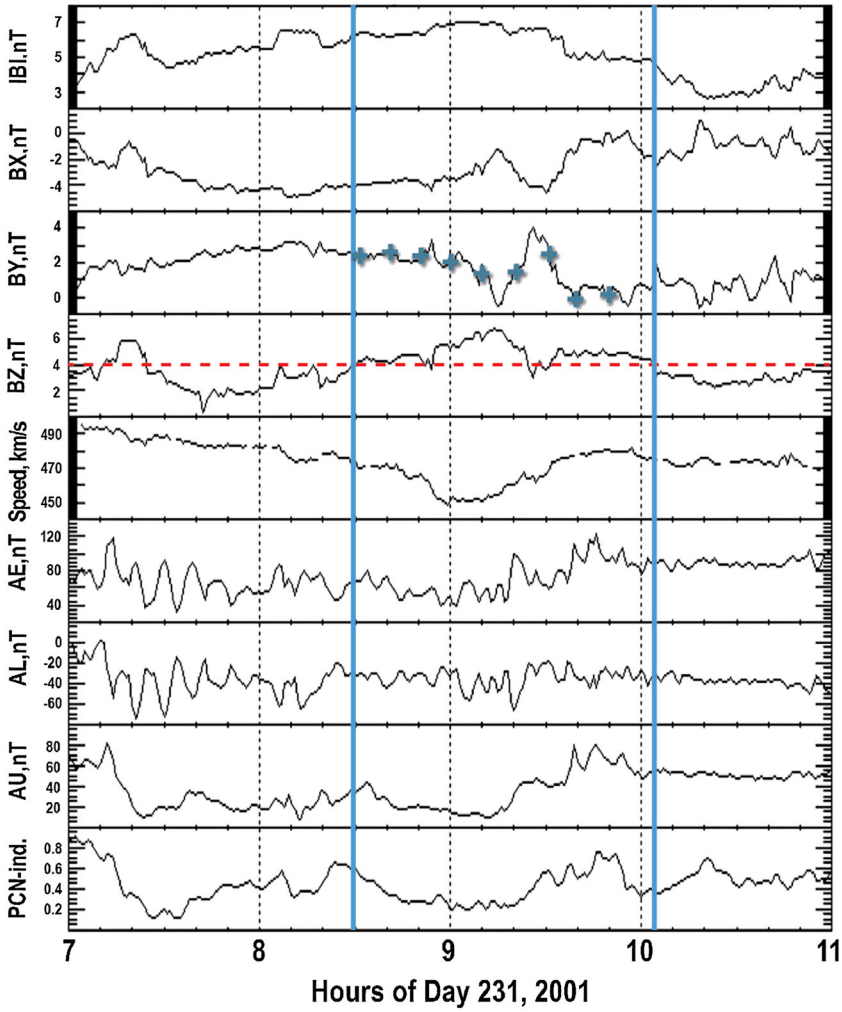

Figure 5. A plot of the 1 min solar wind, interplanetary, and auroral activity data obtained from the NASA OMNIWeb (http://omniweb.gsfc.nasa.gov) for 19 August 2001, 0700–1100 UT, covering the times before, during, and after the TMRB interval. The two blue vertical lines mark the TMRB interval observed by Geotail. The black dotted lines indicate the hourly UT intervals. The top five panels are the external magnetospheric driver parameters: the IMF strength; the IMF Bx, By, and Bz components (in GSM); and the solar wind speed, respectively. The blue crosses in the third panel indicate the IMF By values during times when direction-finding analyses in Figure 4 were performed. The red dotted line in the fourth panel marks the IMF Bz = 4 nT level, which may be regarded as a threshold for the observed TMRB emission (0830–1006 UT). The lower four panels show the geomagnetic (magnetospheric) response parameters: AE, AL, AU, and PC indices.

shown in the second panel in Figure 5) [e.g., *Kessel et al*., 1996; *Luhmann et al*., 1984] and could potentially provide a high-latitude free-energy source to produce the TMRB. The IMF Bz profile shown in Figure 5 (fourth panel) indicates a steady increase of the Bz component starting from well before the TMRB event, to exceeding a Bz value of +4 nT at the start of the event at 0830 UT (marked by first blue vertical line in Figure 5), and to a level of >+6 nT at 0905–0915 UT when the peak TMRB emission was observed simultaneously by IMAGE and Geotail (see Figure 2). After the peak, the Bz component then decreases, dipping momentarily below 4 nT just before 0930 UT, but recovers shortly afterward to a relatively constant level of ~5 nT before dropping below 4 nT again (marked by the second blue line in Figure 5) shortly after 1000 UT when the TMRB also disappears (Figure 2). It should be noted that the momentary Bz dip below 4 nT near 0926 UT corresponds remarkably well to a temporary decrease in the TMRB intensity seen at the same time in the IMAGE observation shown in Figure 2. Thus, treating IMF Bz ~+4 nT as a possible threshold condition for this event, the start, stop, and temporary weakening of the TMRB emission (Figure 2) can all be essentially accounted for by the corresponding variations of the IMF Bz component (Figure 5).

[20] We should note here that in addition to the TMRB interval, Figure 5 shows another small interval near 0720 UT when the IMF Bz component exceeded 4 nT. Yet neither Geotail nor IMAGE detected any TMRB emission at that time (see Figure 2). The lack of TMRB observation at that time may be due to perhaps different plasma conditions at the source or unfavorable spacecraft observing locations for this time.

4.2. Auroral Conditions

[21] The lower four panels in Figure 5 show the geomagnetic (magnetospheric) response parameters: AE, AL, AU, and polar cap (PC) indices, which show no remarkable substorm activity (e.g., AE < 120 nT) during this entire interval. Nevertheless, auroral kilometric radiation (AKR) was present at the beginning and the second half of the TMRB interval. Referring to the panels in Figure 5 for the AE, AL, and PC indices, we notice that those indices exhibit peak levels around 0700, 0820, and 0930–0950 UT, consistent with the times of AKR activations shown in Figure 2. On the other hand, Figure 5 shows no apparent auroral activation during the majority of times (0835–0920 UT) when the TMRB is strongest. It would seem then that there is not a strong association between TMRB and AKR (or auroral activity) as the two emissions at different frequency ranges are clearly not directly correlated. Figure 2 suggests that TMRB tends to occur after AKR activation, when any auroral activity enhancements (in indices) would have subsided.

5. Comparisons of TMRB With Known TMR Components

[22] The TMRB appeared in the same wavelength band (10–100 km) as other TMR. The most notable ones are the different forms of continuum radiation [e.g., *Green and Fung*, 2005; *Grimald et al*., 2008; *Grimald et al*., 2011] and the AMR [*Hashimoto et al*., 1998]. We now compare the observed characteristics of TMRB against the known terrestrial emissions to see whether the TMRB might be a distinct emission.

5.1. Nonthermal Continuum

[23] Classical NTC radiation usually appears as banded emission that extends several hours in the post-midnight to afternoon local times [*Gurnett*, 1975; *Gough*, 1982; *Green and Boardsen*, 1999; *Menietti et al*., 2005]. In addition, trapped NTC at frequencies below the magnetopause plasma frequency (~ 30 kHz) typically appears as a smooth, broadband emission due to the radiation having undergone multiple reflections within the magnetosphere [*Gurnett*, 1975; *Green and Fung*, 2005]. On the other hand, the simultaneous observations of the broadband TMRB (extending well above 30 kHz) by IMAGE and Geotail over widely different longitude and latitude ranges, shown in Figures 1–3, suggest that the TMRB is episodic in time, lasting only ~90 min.

[24] Using ray-tracing calculations, *Green and Boardsen* [1999] showed that NTC is primarily confined to low latitudes, and raypaths reflected off the magnetopause can rarely pass over the polar region at $Z > 5$ *Re*. While these results are consistent with Geotail's position during the TMRB observation, spectral differences from the NTC and the detection of TMRB by IMAGE at high altitude ($Z > 7$ *Re*) over the high-latitude region (see Figure 1) thus make the TMRB likely to be an emission distinct from the classical NTC.

5.2. Continuum Enhancement

[25] CEs are episodic NTC intensity enhancements that can last up to ~2 h [*Kasaba et al*., 1998]. First identified in GEOS 2 data taken in the geosychronous region near midnight [*Gough*, 1982], and then in IMP 6 observations in the magnetotail [*Filbert and Kellogg*, 1989], CE is characterized by a sudden intensification at 15–30 kHz that is followed by an overall broadening to higher frequencies and separating into discrete frequency bands (see Figure 3 in *Gough* [1982]). The band separations also widen with time. Although the TMRB and CE tend to have similar temporal behavior, the TMRB spectral appearance differs significantly from CE by lacking the distinctive frequency bands. Instead, the upper frequencies and cutoff of the TMRB exhibit some systematic or coherent, low-frequency undulations that are clearly visible toward the end of the burst (Figure 3).

[26] Onsets of CE are known to temporally correspond to increases in auroral activity (AE, AU, and AL), including AKR [*Filbert and Kellogg*, 1989; *Kasaba et al*., 1998]. As shown in Figure 2, AKR and TMRB do not have matching start times. The times of increases in auroral indices in Figure 5 are also inconsistent with the beginning time of the TMRB. Despite the similarities in temporal behavior and the compact spectral appearances in the TMRB and the main CE component, the two emissions are not likely to be the same phenomenon.

5.3. Kilometric Continuum

[27] The episodic character of the TMRB (Figure 2) indicates that the TMRB beam (either the nightside beam detected by Geotail or the dayside beam detected by IMAGE) may also be confined in latitude and/or longitude (see section 6), depending on the emission mechanism and the plasma environment in which it operates. Such a

situation may be similar to the KC radiation in that the emitted radiation is limited in latitude and confined in longitude by the plasma surrounding the source [*Green et al*., 2004], but that might be the only similarity between the two emissions. Observed at all local times, KC is known to be generated from deep inside plasmaspheric notches that rotate with the plasmasphere. The narrow latitudinal emission cone of KC (within $\pm 15^\circ$ of the magnetic equator) [*Green et al*., 2004; *Hashimoto et al*., 2006; *Boardsen et al*., 2008] can lead to different spectral appearances in the observations of satellites having different orbital characteristics. First identified in Geotail observations in a near equatorial orbit [*Hashimoto et al*., 1999], KC appeared as discrete frequency bands lasting several hours due to the nearly synchronous changes in the emission-cone and spacecraft local times [*Green et al*., 2002, 2004], see Figure 2.3 in *Hashimoto et al*. [2006]. On the other hand, the polar-orbiting IMAGE satellite often observed KC upon crossing the magnetic equator as discrete-banded emissions with durations inversely related to the observed frequency (e.g., see Figure 2 in *Green and Boardsen*, [2006]). With the emission frequencies extending up to ~800 kHz, the emission band durations change from several hours at low frequencies (consistent with Geotail observations) to less than an hour at high frequencies, yielding a characteristic Christmas-tree spectral pattern. The very similar timing, frequency extents, and spectral shapes of the TMRB observed by Geotail and IMAGE from very different vantage points (Figure 2) mean that the TMRB reported here is distinct from KC.

5.4. NTC Patches

[28] *Grimald et al*. [2011] recently reported CLUSTER observations of NTC patches, which they further classify into (1) plasmaspheric patches consisting of banded emissions that are only observed apparently when the observing spacecraft is close to the plasmaspheric source of the emission and (2) magnetospheric patches that are nonbanded and seem to come from the outer magnetosphere. Like the TMRB shown in Figure 2, NTC patches are episodic but also seem to have durations (~40 min) about one-half to one-third of that of the TMRB (~100 min). Although the IMAGE spectrogram, which is partially contaminated by solar type III emission, seems to suggest the presence of band structure within the TMRB emission, no such structure is visible in the Geotail observations. The lack of banded spectral structure and evidence of any nearby plasmapause density gradients in Figures 2 and 3 indicate strongly that the TMRB is unrelated to plasmasheric patches. Moreover, the simultaneous observations of the TMRB by IMAGE and Geotail at widely different latitudes, longitudes, and radial distances far from any equatorial sources suggest that TMRB might be more comparable, if at all, to the magnetospheric patches reported by *Grimald et al*. [2011].

[29] The statistical results on the outer magnetospheric patches presented by *Grimald et al*. [2011] show that patches account for about 24.4% of all the included (818) outer magnetospheric NTC events observed by CLUSTER. Most outer magnetospheric patches (89%) also have central frequency <40 kHz, similar to that of the TMRB (~20 kHz) being discussed in this paper (Figure 2). It is not clear at the present, however, as to whether the TMRB being discussed here is the same phenomenon as the outer magnetospheric patch. We elaborate in more details below.

5.5. Auroral Myriametric Radiation

[30] The AMR, first discussed by *Hashimoto et al*. [1994], gets its name because it occurs coincidently with AKR and substorm onsets. This emission is believed to be generated in the L-O mode above the local plasma frequency (f_{pe}) in auroral density cavities where the local electron gyrofrequency $f_{ce} > f_{pe}$. The difference in f_{ce} and f_{pe} naturally explains the difference in AKR and AMR frequency ranges [*Hashimoto et al*., 1998]. Although AMR beaming can potentially account for the nightside TMRB observation by Geotail, it could not easily explain the dayside observation at high latitude by IMAGE. The typically high temporal correlation between AMR and AKR makes AMR an unlikely candidate for the observed TMRB (Figure 2).

6. Discussion

[31] An emission named here as a TMRB has been identified based on its frequency range and the simultaneously on-off appearance (like a light bulb) in the dynamic spectrograms (Figure 2) obtained on 19 August 2001 by both the IMAGE and Geotail satellites. During the TMRB observations, the two satellites were widely separated in latitude and longitude (local times), with IMAGE being slight closer to Earth (~7 *Re* altitude) in the afternoon high-latitude magnetosphere and Geotail being slightly farther from Earth (altitude ~8 *Re*) in the pre-dawn/post-midnight sector closer to the magnetic equator (Figure 1). Results from comparing the TMRB with all known TMR components suggest that it may be an emission having a source that is distinct from the plasmasphere. Below we discuss the TMRB occurrence and beaming characteristics and a possible source generation scenario.

6.1. Occurrence

[32] The simultaneous observations of the TMRB by IMAGE and Geotail, as shown in Figure 2, while fortuitous, are an important aspect of the event identification, as simultaneous observations by more than one spacecraft are necessary for establishing the time coincidence and similarities in spectral signatures of the event. The fact that the reported event seems to be the only one found so far during the IMAGE and Geotail common operational interval (2001–2005) suggests that multisatellite observations of TMRB could understandably be a rare occurrence. It actually requires quite stringent combination of solar wind and magnetospheric conditions as well as coordination of multiple satellite positions to detect the TMRB beams simultaneously in widely different directions.

[33] Single-satellite observations of TMRB are certainly possible. Although a few possible events have indeed been found in single-spacecraft observations, they cannot be readily identified as TMRB without the simultaneous observations from different locations to confirm their temporal signatures. Similarly, of the over 800 outer magnetospheric patches identified by *Grimald et al*. [2011] in the 2003 observations by CLUSTER (see section 5.4), some could actually be TMRB*s*. A single observation of a patchy emission, however, might be due to a brief excursion of a satellite track through an otherwise steady emission pattern. Without corroborating observations from widely separated spacecraft, it would be difficult to determine which, if any, of the outer magnetospheric patches were actually TMRB*s*.

[34] In addition, *Grimald et al*. [2011] suggested that the outer magnetospheric patches might be the results of propagation. These authors postulated that nonbanded patch signature could arise from interaction of waves coming from several NTC sources located in different places in the plasmapause density gradient. The observed characteristics of the TMRB clearly indicate, however, that the emission is temporal by nature (as shown by Figure 2) and is beamed directly from a well-defined source as evident by the presence of spin modulations (Figure 3). The high degree of coherence and similarity between the simultaneous IMAGE and Geotail observations (Figure 2) argues against the TMRB being the sum of radiation from multiple NTC sources. Moreover, for an NTC source in the plasmapause (with appropriate density gradient) to be detected directly by Geotail, it would have to be located on the nightside near the magnetic equator, but it would be difficult for the same source to beam radiation simultaneously to the high-latitude IMAGE location on the dayside without being blocked or diverted by the intervening plasmasphere. Therefore, the observed TMRB characteristics are inconsistent with the origin of the outer magnetopsheric patches as postulated by *Grimald et al*. [2011], or the two types of emissions are distinct from one another.

6.2. Beaming Characteristics

[35] The presence of spin modulations in the TMRB signals (Figure 3) implies that the radiation detected by Geotail must have discrete, well-defined, propagation directions from one time to the next as shown in Figure 4. In conjunction with the simultaneous observation by IMAGE at the nearly diametrically opposite high-latitude location (Figure 1), the restriction of TMRB observations to a small discrete range of propagation directions suggests that the TMRB source may be a temporally active, central source having either an isotropic or a fan-beam radiation pattern as discussed earlier. In either case, a compact (narrowly distributed) source located earthward of Geotail is implied because an extended source with appreciable spatial structures would otherwise produce radiation with mixed propagation directions leading to little or no spin modulation.

[36] We note that the time interval over which the TMRB (or any radiation phenomenon) is observed by a satellite is determined by two factors: (1) the length of time when the emission mechanism is active or operational, and (2) the amount of time a satellite remains within the radiation beam. Based on the sensitivity of the TMRB emission on the variability of IMF Bz and the possible threshold condition of IMF Bz = 4 nT (see the fourth panel in Figure 5), it seems that the Geotail observations might have actually captured the entire TMRB emission interval, 0830–1006 UT. The shorter IMAGE TMRB interval (both in time and frequency range) thus implies that the IMAGE satellite must have transited across the entire dayside TMRB beam more quickly.

[37] During the shorter IMAGE TMRB interval (0832–0952 UT), the geomagnetic latitude and longitude of IMAGE increased by 7.4° and 6.0°, respectively. Its magnetic local time also increased from 15:29 to 17:11; that is, IMAGE actually moved duskward even though its GSM longitude remained relatively fixed (Figure 1). On the other hand, during the longer Geotail TMRB interval, the geomagnetic latitude of Geotail increased only by ~4.5°, while its geomagnetic longitude decreased by ~6.5° during the TMRB interval. During that time, Geotail's magnetic local time increased from ~3:10 to ~4:10 as depicted in Figure 4. The dawnward motion of Geotail might have helped keep Geotail in the TMRB radiation beam at the time when the TMRB source was apparently also moving toward earlier local times (see Figure 4). The difference in the lengths of the IMAGE and Geotail TMRB intervals can thus be understood in terms of the difference in the amount of time it took the two satellites to transit the limited local time or longitudinal extent of TMRB beams.

[38] An attempt was also made to investigate the angular extent of the TMRB beam by seeing if other satellites with radio receivers (Wind, CLUSTER, Akebono, and FAST) might also have detected the event in Figure 2 in different directions. During the times of Figure 2, e.g., at ~0900 UT when the TMRB event appeared to be strongest with the broadest frequency extent, the Wind spacecraft was located far upstream in the southern hemisphere ($X_{GSM} = 50$ *Re*, $Y_{GSM} = 191$ *Re*, $Z_{GSM} = -93$ *Re*) where it detected no evidence of the TMRB event despite the fact that the highest frequencies (~ 60 kHz) of the TMRB emission could well have escaped the magnetosphere and reached the Wind spacecraft. The CLUSTER 1–4 satellites, on the other hand, were all located in the nightside northern hemisphere ($X_{GSM} \sim -13.4$ *Re*, $Y_{GSM} \sim -2.1$ *Re*, $Z_{GSM} \sim 9.6$ *Re*), but unfortunately, no data were collected by the CLUSTER WHISPER instrument during this time. Similarly, the VLF receiver on the Japanese Akebono satellite ($X_{GSM} = -0.73$ *Re*, $Y_{GSM} = -0.14$ *Re*, $Z_{GSM} = -1.41$ *Re*) did not operate on the day of interest (Y. Goto, private communications, 2010), so no radio data were available from Akebono. Finally, the low-altitude FAST satellite detected no electromagnetic radiation in the TMRB frequency range (10–50 kHz) at 9:10 UT when the satellite was traversing the southern plasmasphere ($X_{GSM} = -0.67$ *Re*, $Y_{GSM} = -0.74$ *Re*, $Z_{GSM} = -1.19$ *Re*) where the local high plasmaspheric densities would have prevented the observation of the radiation. While there seems to be no broad-based evidence for the presence or absence of an isotropic beam, the lack of TMRB observations by the Wind satellite was at least consistent with the TMRB radiation beam having limited azimuthal or meridional distributions.

[39] Finally, we note that despite the slow orbital motions of Geotail (Figure 1), Figure 4 shows an apparent, systematic migration of the source directions or positions to earlier local times over the 80 min interval for which spin-modulation analyses were performed. The apparent azimuthal source motion is consistent with the TMRB source being a compact source. In addition, we notice also that there is a remarkable dependence of the apparent azimuthal position of the TMRB source on the IMF By component during the TMRB interval.

[40] The crosses in the third panel of Figure 5 mark the IMF By values at the nine time steps at which direction-finding analyses were performed. With the exception of step 7 (9:30 UT) when the IMF By component increased rather abruptly back to ~3 nT, the IMF By components for the rest of the eight time steps tend to decrease monotonically from ~3 nT at 8:30 UT (step 1) to nearly ~0 nT at 9:50 UT (step 9). Figure 4 shows the apparent migration of the corresponding source directions, slowly with IMF By (and time), toward earlier local times as described earlier. At step 7 (9:30 UT), however, there was a sudden, temporary return of the TMRB source direction back toward those in steps

1 and 2. This change in source azimuthal directions seems to coincide with the sudden, temporary increase in IMF By. With the sequence of spin-modulation indices M determined above, we can also estimate the corresponding TMRB source elevation angles, Λ_{GSE}, above the Ecliptic (the approximate antenna spin plane) as seen from Geotail by using the expression $|\cos(\Lambda_{GSE})|^2 = 2M/(1+M)$ [*Menietti et al.*, 1998; J. D. Menietti, private communications, 2012] and obtain the $|\Lambda_{GSE}| = 11.0$, 15.9, 25.4, 22.6, 23.3, 30.0, 43.3, 36.9, and 31.5, respectively, for the different time steps.

6.3. Possible Source and Generation Mechanism

[41] As previously discussed, it would be difficult for an equatorial source in the plasmapause to beam radiation directly to both the Geotail and IMAGE locations simultaneously; the only other source location that could produce radiation at the TMRB frequencies (10–60 kHz) is likely to be along the dayside cusp field lines. Without polarization information, however, the TMRB could be either R-X or L-O mode radiation.

[42] Using a centered-dipole magnetic field model and a composite density model given by the sum of a plasmasphere, PC, and the cusp, we have computed the 20, 40 and 60 kHz contours of the L-O mode cutoff or electron plasma frequency (Figure 6, upper panel) and R-X mode cutoff frequency (lower panel), in an approximate meridional plane containing both the IMAGE and Geotail positions during the TMRB interval. The plasmasphere model parameterized by Kp is that of *Gallagher et al.* [1988]. The PC density model, which has no parameterization, is that of *Persoon et al.* [1983]. The shape of the magnetopause, parameterized by solar wind dynamic pressure and IMF Bz, is given by *Roelof and Sibeck* [1993]. The density along the magnetopause surface is that of the gas dynamic model of *Spreiter et al.* [1966]. The ad hoc cusp density model is for illustrative purposes only and should not be used for detailed quantitative analysis.

[43] The location of the cusp center is given by the Earth-centered dipole magnetic field line whose invariant latitude in 80° at noon MLT, consistent with the statistical cusp location given in *Fung et al.* [1997]. The cusp density along the cusp center is assumed to be the magnetopause density at the MLT location where this line intersects the magnetopause. The density profile across the cusp is assumed to drop off exponentially from the cusp center with a half-width in invariant latitude of 1° and in magnetic local time of 3 h. Based on such simplified models, Figure 6 shows that a source located at some altitude on the poleward edge of the cusp field lines has the potential of sending radiation at the observed TMRB frequency ranges to both IMAGE and Geotail simultaneously without obstruction. In order for the radiation to propagate across the polar region, an R-X mode source would need to be situated at a higher altitude than an L-O mode source.

[44] The TMRB characteristics—(1) dayside source located along poleward edge of cusp field lines, (2) correlation with northward IMF Bz, and (3) variation of source local times with IMF By—are reminiscent of those associated with dayside cusp reconnection [e.g., *Kessel et al.*, 1996; *Luhmann et al.*, 1984]. Consequently, we postulate that the energetic electrons produced in the reconnection process might be a source for the TMRB. This postulate seems reasonable because it naturally accounts for all the observed TMRB characteristics and their IMF dependencies.

[45] We should further point out that while a complete analysis is beyond the scope of this paper, the TMRB observations by Geotail do provide further clues for testing the postulated source scenario. Throughout the TMRB interval, even though the geomagnetic latitude of Geotail increased by 4.5°, its GSE latitude actually remained relatively constant (changing only from ~−9° to ~−10°). Since the Geotail antenna spin plane is nearly aligned (within ~3°) with the Ecliptic (GSE X-Y) plane, the decreasing modulation indices described above suggest that the compact TMRB source must have gained $|\Lambda_{GSE}|$ while moving toward earlier local times during the TMRB interval. By relating the source motions to dayside merging processes, such as those discussed by *Crooker* [1979] and *Luhmann et al.* [1984], one can investigate the TMRB source scenario. If the postulate turns out to be correct, then the TMRB would be a first report of radiation signature resulting from magnetic merging or reconnection processes in geospace plasma.

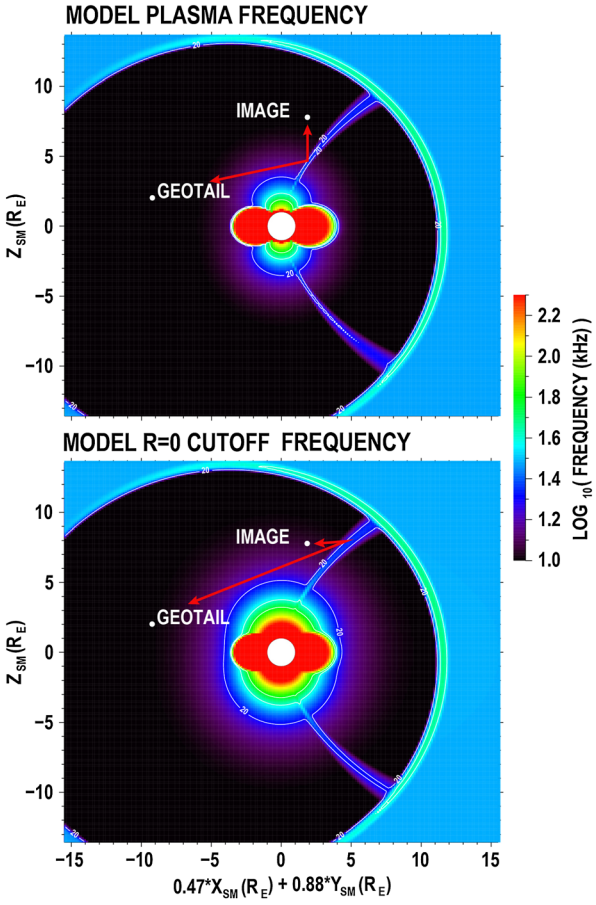

Figure 6. Plots of the plasma-frequency (upper) and $R = 0$ (lower) cutoff in an approximate meridional plane, given by $0.47X_{SM}(R_E) + 0.88Y_{SM}(R_E)$, that contains both the Geotail and IMAGE positions (see Figure 1) during the TMRB event shown in Figure 2. The white contours are successively at 20, 40, and 60 kHz. The panels show that the poleward edge of the cusp field lines might be a potential TMRB source location for either R-X or L-O mode waves.

7. Summary and Conclusions

[46] We report the simultaneous observations of a TMRB by Geotail and IMAGE from very different vantage points (Figure 1). The similarities in timing, frequency extents (12–60 kHz), and spectral characteristics of the TMRB seen by the two spacecraft (Figure 2) imply that the TMRB was a temporal emission with possibly a fan beam radiation pattern emitted from a discrete source. The TMRB upper cutoff frequencies clearly exhibit undulations as shown in Figure 3. Similar undulations also appear in the lower cutoff frequencies, particularly toward the end of the burst after 0940 UT in Figure 3. Such variability could be related to density increases and decreases associated with field-aligned density irregularities (FAI) seen across magnetic field lines. For example, assuming L-O mode propagation, the undulating change in the upper TMRB cutoff frequency of $\Delta f \sim 5$ kHz at $f \sim 50$ kHz (near 0950 UT in Figure 3) corresponds to a change in electron density of $\Delta n/n \sim 5\%$, which seems reasonable and consistent with typical density fluctuation levels associated with FAI in the plasmasphere [*Fung et al*., 2003; *Fung and Green*, 2005].

[47] The TMRB emission seems to occur only after AKR activation as shown in Figures 2 and 5, so its occurrence might be only subsequent or unrelated to auroral activity. On the other hand, the dayside cusp source location implied by beaming considerations as well as the apparent association with positive IMF Bz condition and correlation with IMF By component throughout the TMRB interval (Figure 5) suggest that magnetic merging occurring over a limited region poleward of the cusp could provide a transient, high-latitude free-energy source for the TMRB, which was fortuitously observed simultaneously by IMAGE and Geotail at diametrically opposite locations (Figure 1). This is consistent with the compactness of the observed TMRB emission pattern.

[48] Comparisons of TMRB characteristics against all other known TMR components reveal that the TMRB was likely a distinct emission, although the emission mechanism might still be similar to those responsible for generating the NTC, CE, KC, or AMR. The TMRB may thus be beamed radiation resulting from linear [e.g., *Jones*, 1976, 1982; *Grimald et al*., 2008] or nonlinear mode-conversion mechanisms [e.g., *Fung and Papadopoulos*, 1987], consistent with the spin modulations seen by Geotail. Further research on TMRB propagation and source mechanism will be important to confirm its characteristics and source scenario. Further work we plan to perform will include searching various wave data bases for additional events, performing ray-tracing modeling to validate potential source regions, and modeling of the TMRB source region.

[49] **Acknowledgments.** We gratefully acknowledge the SSCWeb and OMNIWeb services provided by the NASA Space Physics Data Facility and the use of the OMNI data sets. We greatly appreciate the referees' thorough reading and many suggestions that helped improve the paper.

References

Boardsen, S. A., J. L. Green, and B. W. Reinisch (2008), Comparison of kilometric continuum latitudinal radiation patterns with linear mode conversion theory, *J. Geophys. Res.*, *113*, A01219, doi:10.1029/2007JA012319.

Crooker, N. U. (1979), Dayside Merging and Cusp Geometry, *J. Geophys. Res.*, *84*, 951–959.

Fainberg, J. (1979), Technique to Determine Location of Radio Sources from Measurement Taken on Spinning Spacecraft, *NASA Technical Memorandum* 80598, NASA Goddard Space Flight Center, Greenbelt MD, November.

Filbert, P. C., and P. J. Kellogg (1989), Observations of low frequency radio emissions in the Earth's magnetosphere, *J. Geophys. Res.*, *94*, 8867.

Fung, S.F., and K. Papadopoulos (1987), The emission of narrowband/narrow band Jovian kilometric radiation, *J. Geophys. Res. 92*, 8579–8593.

Fung, S. F., and J. L. Green (2005), Modeling of field-aligned guided echoes in the plasmasphere, *J. Geophys. Res.*, *110*, A01210, doi:10.1029/2004JA010658.

Fung, S. F., R. F. Benson, D. L. Carpenter, J. L. Green, V. Jayanti, I. A. Galkin, and B. W. Reinisch (2003), Guided echoes in the magnetosphere: Observations by Radio Plasma Imager on IMAGE, *Geophys. Res. Lett.*, *30*(11), 1589, doi:10.1029/2002GL016531.

Fung, S. F., T. E. Eastman, S. A. Boardsen, and S.-H. Chen (1997), High-altitude cusp positions sampled by the Hawkeye satellite, *Phys. Chem. Earth*, *22*, 653–662.

Gallagher, D.L., P.D. Craven, and R.H. Comfort (1988), An empirical model of the earth's plasmasphere, *Adv. Space Res.*, *8*, 15.

Gough, M.P. (1982), Nonthermal continuum emissions associated with electron injections: Remote plasmapause sounding, *Planet. Space Sci.*, *30*, 657.

Green, J. L., and S. Boardsen (1999), Confinement of nonthermal continuum radiation to low latitudes, *J. Geophys. Res.*, *104*, 10,307–10,316.

Green, J. L., and S. Boardsen (2006), Kilometric continuum radiation, *Radio Sci. Bull.*, URSI, *318*, 34–42.

Green, J. L., and S. F. Fung (2005), Advances in Inner Magnetospheric Passive and Active Wave Research, in Physics and Modeling of the Inner Magnetosphere, pp. 37–54, Geophysical Monogr. 155, AGU, Washington D.C., doi:10.1029/155GM21.

Green, J. L., B. R. Sandel, S. F. Fung, D. L. Gallagher, and B. W. Reinisch (2002), On the Origin of Kilometric Continuum, *J. Geophys. Res.*, *107* (A7), 1105, doi:10.1029/2001JA000193.

Green, J. L., S. Boardsen, S. F. Fung, H. Matsumoto, K. Hashimoto, R. R. Anderson, B. R. Sandel, and B. W. Reinisch (2004), Association of kilometric continuum radiation with plasmaspheric structures, *J. Geophys. Res.*, *109*, A03203, doi: 10.1029/2003JA010093.

Grimald, S., P. M. E. Decreau, P. Canu, A. Rochel, and X. Vallieres (2008), Medium-latitude sources of plasmaspheric nonthermal continuum radiations observed close to harmonics of the electron gyrofrequency, *J. Geophys. Res.*, *113*, A11216, doi:10.1029/2008JA013290.

Grimald, S., F. El-Lemdani-Mazouz, C. Foullon, P. M. E. Décréau, S. A. Boardsen, and X. Vallières (2011), Study of nonthermal continuum patches: Wave propagation and plasmapause study, *J. Geophys. Res.*, *116*, A07219, doi:10.1029/2011JA016476.

Gurnett, D. A. (1975), The Earth as a radio source: The nonthermal continuum, *J. Geophys. Res.*, *80*, 2751–2763.

Hashimoto, K., H. Matsumoto, H. Kojima, T. Murata, I. Nagano, T. Okada, K. Tsuruuda, and T. Iyemori (1994), Auroral myriametric radiation observed by Geotail, *Geophys. Res. Lett.*, *21*, 2927–2930.

Hashimoto, K., S. Kudo, and H. Matsumoto (1998), Source of auroral myriametric radiation observed with Geotail, *J. Geophys. Res.*, *103*, 23475–23483.

Hashimoto, K., W. Calvert, and H. Matsumoto (1999), Kilometric continuum detected by GEOTAIL, *J. Geophys. Res.*, *104*, 28,645–28,656.

Hashimoto, K., J. L. Green, R. R. Anderson, and H. Matsumoto (2006), Review of Kilometric continuum, in Geospace Electromagnetic Waves and Radiation, edited by J. W. LaBelle, and R. A. Treumann, Lecture Notes in Physics, vol. 687, pp. 37–54, Springer, Berlin.

Jones, D. W. (1976), Source of terrestrial nonthermal continuum radiation, *Nature*, *260*, 686–689.

Jones, D. (1982), Terrestrial myriametric radiation from the earth's plasmapause, *Planet. Space Sci.*, *30*, 399.

Kasaba, Y., H. Matsumoto, K. Hashimoto, R. R. Anderson, J.-L. Bougeret, M. L. Kaiser, X. Y. Wu, and I. Nagano (1998), Remote sensing of the plasmapause during substorms: GEOTAIL observation of nonthermal continuum enhancement, *J. Geophys. Res.*, *103*, 20389–20405.

Kessel, R. L., S.-H. Chen, J. L. Green, S. F. Fung, S. A. Boardsen, L. C. Tan, T. E. Eastman, J. D. Craven, and L. A. Frank (1996), Evidence of high-latitude reconnection during northward IMF: Hawkeye observations, *Geophys. Res. Lett.*, *23*, 583–586.

Luhmann, J.G., Walker, R.J., Russell, C.T., Crooker, N.U., Spreiter, J.R., and Stahara, S.S. (1984). Patterns of potential magnetic field merging sites on the dayside magnetopause, *J. Geophys. Res.*, *89*(A3), doi:10.1029/0JGREA0000890000A3001741000001.

Matsumoto, H., I. Nagano, R. R. Anderson, H. Kojima, K. Hashimoto, M. Tsutsui, T. Okada, I. Kimira, Y. Omura, and M. Okada (1994), Plasma wave observations with *GEOTAIL* spacecraft, *J. Geomagn. Geoelectr. 46*, 59.

Menietti, J. D., O. Santolik, J. S. Pickett, and D. A. Gurnett (2005), High resolution observations of continuum radiation, *Planet. Space Sci.*, *53*, 283–290, doi:10.1016/j.pss.2004.09.054.

Menietti, J. D., D. A. Gurnett, W. S. Kurth, J. B. Groene, and L. J. Granroth (1998), Galileo direction finding of Jovian radio emissions, *J. Geophys. Res.*, *103*, 20,001–20,010.

Persoon, A. M., D. A. Gurnett, and S. D. Shawhan (1983), Polar cap electron densities from DE 1 plasma wave observations, *J. Geophys. Res.*, *88*, 10,123–10,136.

Reinisch, B. W., et al. (2000), The Radio Plasma Imager investigation on the *IMAGE* spacecraft, *Space Sci. Rev.* special issue on the IMAGE mission, *91*, 319–359.

Roelof, E. C., and D. G. Sibeck (1993), Magnetopause shape as a bivariate function of interplanetary magnetic field Bz and solar wind dynamic pressure, *J. Geophys. Res.*, *98*, 21,421–21,450. (Correction, *J. Geophys. Res.*, 98, 21,499.)

Scarf, F. L., G. M. Crook, I. M. Green, and P. F. Virobik (1968), Initial results of the Pioneer 8 VLF electric field experiment, *J. Geophys. Res.*, *73*, 6665–6686.

Spreiter J. R., A. L. Summers, and A. Y. Alksne (1966), Hydromagnetic flow around the magnetosphere, *Planet. Space Sci.*, *14*, 223–253.